Nanoscale

COMMUNICATION

View Article Online
View Journal | View Issue

Porous titanium oxynitride sheets as electrochemical electrodes for energy storage†

Cite this: *Nanoscale*, 2014, **6**, 5106

Received 7th January 2014
Accepted 7th March 2014

DOI: 10.1039/c4nr00101j

www.rsc.org/nanoscale

Ting-Ting Chen,[a] Hsiao-Ping Liu,[a] Yen-Ju Wei,[b] I-Chun Chang,[a] Min-Han Yang,[a] Yu-Shu Lin,[a] Kuei-Lin Chan,[a] Hsin-Tien Chiu[b] and Chi-Young Lee*[a]

A flexible, porous TiO_xN_y sheet consisting of numerous conductive fibers was synthesized by nitridation of titanate and further used as an electrochemical electrode. The high surface area and mixed-oxidation state of titanium make TiO_xN_y sheets to be promising candidates for a good supercapacitor.

As a novel material developed recently, titanium oxynitride, TiO_xN_y ($x + y = 1$), can be regarded as a solid solution of isostructured trivalent TiN (Ti^{3+}) and divalent TiO (Ti^{2+}); meanwhile, its properties can be adjusted by O/N ratios.[1–4] Direct thermal nitridation of TiO_2 in a NH_3 atmosphere has been widely adopted to produce TiO_xN_y and TiN.[1–7] Nitridation is a diffusion-controlled reaction, and its corresponding conversion mechanism has received considerable attention.[1–4,7] The five-coordinated Ti^{4+} site on the surface with a nature of Lewis-acid can be regarded as the active site for anchoring NH_3 molecules. The NH_3 decomposition and O/N atom replacement lead to the conversion from TiO_2 into $TiO_{2-x}N_x$ (N-doped TiO_2) and eventually into TiO_xN_y and TiN. The various applications of TiO_xN_y and TiN as electrochemical electrodes include their use in supercapacitors,[8–14] lithium ion batteries,[6,15] photoelectrochemical devices[16] and water electrolysis,[3] owing to their high electrical conductivity and excellent chemical resistance to acids/alkali.

Recent efforts have focused on achieving porous, large surface area and flexible electrochemical electrodes. Hybrid electrodes were formed by combining nanostructured materials and flexible as well as extra thin substrates (*e.g.*, graphene,[15,17] carbon cloth,[12] and Ni foam[18]). Li *et al.* demonstrated the feasibility of using free-standing TiN nanowires (NWs) on carbon cloth as high-performance and flexible electrodes of supercapacitors.[12] The carbon cloth provides the permeability for the nitridation of TiO_2 NWs and convenience in flexible electronics as well.

This work designs a flexible and conductive TiO_xN_y sheet with the porosity to function as a single material electrochemical electrode. Membrane-like titanate sheets are used as the starting material, since one-dimensional fibers with a length of several micrometers are prone to intertwining with each other during filtration.[19,20] Titanate sheets with a pore size of ~80 nm (macropore) and high gas permeability are feasible for diffusion-controlled nitridation. The titanate sheets are heated at high temperatures (600–800 °C) under an ammonia atmosphere, where the titanate sheets are gradually converted into TiO_xN_y sheets. The evolution of composition and phase transformation significantly affects chemical and physical properties. Moreover, O/N atom replacement creates nanopores (2–15 nm) over fibers during nitridation, whereas the TiO_xN_y sheets still retain macropores. In general, the porosity, conductivity and oxidation state of TiO_xN_y sheets are easily controlled by the O/N ratio during nitridation. Furthermore, the performance of TiO_xN_y sheets in supercapacitors is investigated. Table 1 summarizes the properties and electrochemical behavior of TiO_xN_y sheets.

Free-standing TiO_xN_y sheets were synthesized by a two-step procedure. Further details can be found in the ESI.† The titanate fibers referred to herein as ST were prepared by a hydrothermal reaction and, then, were casted on the membrane during filtration of the ST suspension.[19,20] Next, the fibers were dried in an oven at 50 °C overnight. Thus, a free-standing ST sheet was separated from the filter membrane during water evaporation. According to Fig. S1,† the white ST sheet can be bent freely by hand. The SEM images of ST in Fig. 1a displayed that ST consists of randomly stacked high density fibers with a smooth and glossy surface. Each fiber is several micrometers in length and 40–120 nm in width. During the filtration of the ST suspension, the fibers tend to interlace with each other, subsequently constructing a dense network and providing flexibility to sheets (Fig. S1c†).

[a]*Department of Materials Science and Engineering, National Tsing Hua University, Hsinchu, Taiwan 30043, Republic of China. E-mail: cylee@mx.nthu.edu.tw*

[b]*Department of Applied Chemistry, National Chiao Tung University, Hsinchu, Taiwan 30050, Republic of China. E-mail: htchiu@faculty.nctu.edu.tw*

† Electronic supplementary information (ESI) available. See DOI: 10.1039/c4nr00101j

Table 1 Properties of titanate and TiO_xN_y

Sample	Color	Phase	Lattice constant (Å)	O/N ratio	BET ($m^2\ g^{-1}$)	Conductivity[b] ($S\ cm^{-1}$)	C_{sp}[c] ($F\ g^{-1}$)
ST	White	$H_4Ti_4O_{10}$	—	—	32.2	—	—
N64	Cyan	TiN/TiO[a]	4.1886	4.55	58.9	16.6	120.9
N74	Blue	TiN/TiO[a]	4.1960	2.45	47.8	180.9	88.9
N84	Black	TiN/TiO[a]	4.2239	0.39	24.0	314.5	28.7

[a] TiN and TiO are isostructural. [b] The conductivity was measured using the Hall-effect measurement system. [c] C_{sp} (specific capacitance) was calculated from galvanostatic curves of the samples at a current density of 1.25 A g^{-1} with potential windows ranging from 0 to 0.8 V.

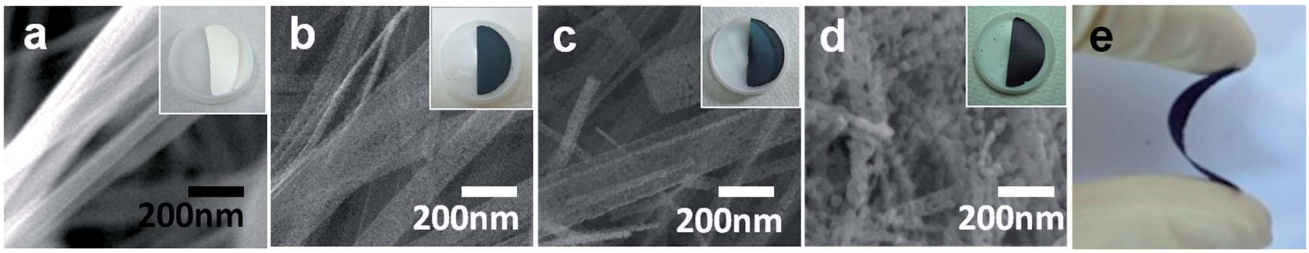

Fig. 1 SEM images (inset: photograph) of the as-synthesized products: (a) ST, (b) N64, (c) N74 and (d) 84. (e) Digital photograph of flexible N84 sheets.

Additionally, the ST sheets were heated under an ammonia atmosphere at different temperatures. Fig. 1b–d display the photographs of N64, N74, and N84 prepared at 600 °C, 700 °C, and 800 °C for 4 h, respectively. After the nitridation, all sheets sustained the flexibility (Fig. 1e), whereas a difference in color was observed. Below 600 °C of thermal treatment, sheets turned from a yellowish to greenish color. With an increasing temperature (>600 °C), the sheets turned from a navy blue to darkish color. The SEM images in Fig. 1b–d display the structure of TiO_xN_y. As the temperature increased, the fibers became short and porous. N64 and N74 still retained the fibrillar texture with tens of micrometers in length, whereas N84 did not exhibit a fiber-like structure (Fig. S2†). As the reaction time was increased from 4 h to 8 h at 800 °C, the fibers collapsed and became a coral-like structure (Fig. S3a,† N88). The TEM images of N64 in Fig. S4†display a rough and porous surface. The nanosized pores (*i.e.* about 2–15 nm) are distributed randomly over the coarse fibers, which correlates well with the SEM observations.

Fig. 2 shows the XRD patterns of TiO_xN_y sheets obtained at different temperatures. All of the TiO_xN_y samples exhibited diffraction peaks at 2θ = around 37.0°, 43.0°, 47.7°, 62.6°, and 74.8°. This correlates with that of cubic structures and is located between the corresponding peaks of TiN (JCPDS 38-1420, a = 4.241 Å) and TiO (JCPDS 08-0117, a = 4.177 Å). Table 1 lists the lattice parameters of TiO_xN_y, which were refined with Celref. The stoichiometric coefficients of these TiO_xN_y were determined by Vegard's law:[2]

$$a_{TiO_xN_y} = xa_{TiO} + ya_{TiN},\ x + y = 1 \quad (1)$$

where $a_{TiO_xN_y}$, a_{TiO} and a_{TiN} refer to the lattice constants of TiO_xN_y, TiO and TiN, respectively. Interestingly, N64 and N74

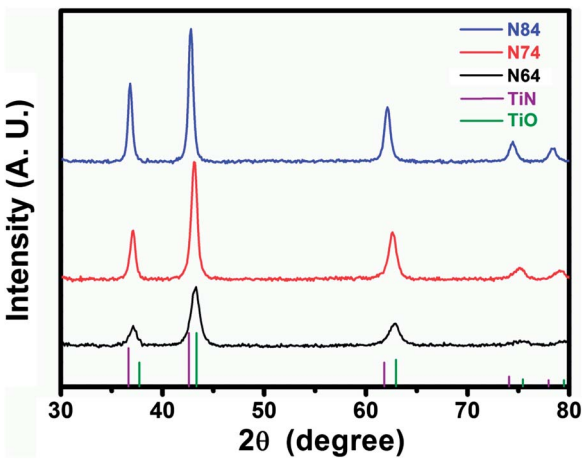

Fig. 2 XRD pattern of TiO_xN_y sheets prepared at various temperatures. For comparison, the purple line denotes TiN (JCPDS 38-1420), and the green line represents TiO (JCPDS 08-0117) standards.

had slightly asymmetric diffraction peaks, especially peaks at 2θ = 37.0° and 47.7° (Fig. S5†). The peak shoulders slanted to a low degree, which correspond to the peaks of TiN. The nitridation process is diffusion limited, so that the nitrogen content of TiO_xN_y continuously decreases on moving away from the surface. This results in a TiN-rich outer layer.

This study also investigated the chemical environments of Ti and N in TiN_xO_y by using XPS, as shown in Fig. S6 and S7,† respectively. Fig. S6† shows the N 1s spectra of TiN_xO_y. The two major peaks, 396.5 and 397.3 eV, appear owing to TiO_xN_y and TiN, respectively, whereas the small peak at 398.5 is an adsorbed N-contained species.[1,2,7] The peak at 397.3 eV increased in intensity with an increasing temperature, whereas the peak at

396.5 eV decreased in intensity. This observation reveals that the amount of Ti–N bonding increased with an increasing nitridation temperature. In Fig. S7†, the Ti $2p_{3/2}$ spectra of TiN_xO_y display three major peaks at 455.6, 457.1, and 458.8 eV, which were assigned to Ti–N, Ti–N–O, and Ti–O respectively.[1,2,7] Similarly, the Ti–N–O peak intensity decreased with respect to the reaction temperature, whereas the intensity of TiN characteristic peaks increased continuously. A higher nitrogen content of TiO_xN_y resulted in more trivalent titanium (Ti^{3+}), leading to a higher oxidation state of TiO_xN_y. For N84, the signal intensity of Ti–N exceeded that of Ti–N–O. The Ti–N bonding (as shown in both Ti 2p and N 1s spectra) indicates the presence of a TiN-rich layer. We can infer that TiO_xN_y eventually converted into pure TiN. However, the detection of Ti^{4+} (Ti–O bonding) was owing to "amorphous TiO_2", which was caused by the exposure of air to the samples just before the XPS measurement (crystalline TiO_2 was not found in the XRD pattern).[1,2,4]

According to the literature, the conductivity of TiO and TiN is approximately 3×10^2 and 2.5×10^6 S cm^{-1}, respectively.[12,21] The conductivity of TiO_xN_y sheets was measured using the Hall-effect measurement system. Increasing the reaction temperature also increased the degree of nitridation, thereby raising the electrical conductivity of the sheets (16.6–314.5 S cm^{-1}). Additionally, the conductivity of TiO_xN_y sheets is also comparable to TiO, yet markedly lower than that of TiN. This difference may be owing to the low stack density of TiO_xN_y. Nevertheless, conductive TiO_xN_y sheets can be considered as an electrical network for the fast charge transport in electrochemical applications.

The porosity of the samples was determined by measuring the nitrogen sorption. Fig. S8a† shows the nitrogen adsorption/desorption isotherms of ST and TiO_xN_y. The pore-size distribution plot reveals the presence of macropores (50–150 nm) in all ST and TiO_xN_y (Fig. 3). Their presence is related to the voids between randomly intertwined fibers in sheets (Fig. S1c†). The macropore size of the sheets normally depends on the size of the precursor fibers.[19,20] We can infer that the sheet remained macroporous after thermal nitridation because the fibers were still interwoven with each other.

However, according to Fig. 3, the pore-size distribution of N64 and N74 shows a bimodal type with mesopores (small pore, <25 nm) and macropores (large pore, 50–150 nm) as well.

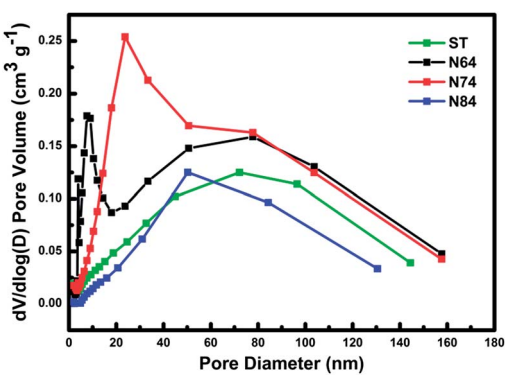

Fig. 3 BJH pore-size distribution curves of samples.

Additionally, the shape of an isotherm with a hysteresis loop belongs to a type IV isotherm, which is associated with two-step capillary condensation in the mesopores (2–50 nm).[22] The presence of mesopores is related to the porous appearance in the fibrillar structure. The nanopores (with a pore size of ~2–15 nm) in N64 are clearly observed in the TEM image (Fig. S4†). BET analysis indicates that the specific surface area of N64 (58.9 m^2 g^{-1}) is the highest among the obtained TiO_xN_y.

The nitridation of titanate has been developed to synthesize TiN_xO_y nanostructures.[1–4] The reaction temperature heavily influences the morphologies of the final products. Earlier studies attribute the conversion of TiN_xO_y to Ostwald ripening crystal growth during nitridation.[4] The decomposition of $NH_{3(g)}$ leads to the formation of active $N_{(ads)}$ at temperatures exceeding 573 K. The active $N_{(ads)}$ replaces O atoms and forms bonds to Ti atoms in titanate as the stable configuration N^{3-}.[1] Replacing O atoms with N atoms from titanate surface creates defects and causes the rough appearance.[4] Moreover, cubic TiO is a highly disordered structure with lattice defects (*i.e.* vacancies of either Ti or O in the defect rock salt structure).[1] During the reaction, the smooth surfaced ST fibers are gradually converted into cubic TiO_xN_y which is highly porous and coarse under the reaction temperature of 600 K. As the decomposition of $NH_{3(g)}$ speeds up with the increase of nitridation temperature (above 800 °C), crystal growth accelerates significantly, resulting in a broken and coral-like structure and vanishing of the nanopores (Fig. S3a†).

As is well known, transition metal nitrides are suitable materials for supercapacitor applications, owing to their excellent electrical conductivity, multi-oxidation state and excellent chemical resistance to acids/alkali.[8–14,23,24] Additionally, this work attempts to understand the electrochemical properties of TiO_xN_y related to their chemical composition by using the conductive TiO_xN_y sheet as a working electrode in 2 M H_2SO_4. Experimental details can be found in the ESI.† Fig. 4a shows the cyclic voltammetric (CV) curves of TiO_xN_y sheets at a scan rate of 30 mV s^{-1}. CV curves display a nearly symmetric rectangular shape in all samples, indicating an electrochemical behavior of typical supercapacitances. Additionally, the current density of TiO_xN_y increases with a decreasing reaction temperature, implying that the degree of nitridation influences the electrochemical behavior of TiO_xN_y. Importantly, N64 yields the highest current density. The approximately linear and symmetrical constant current galvanostatic (GV) curves further

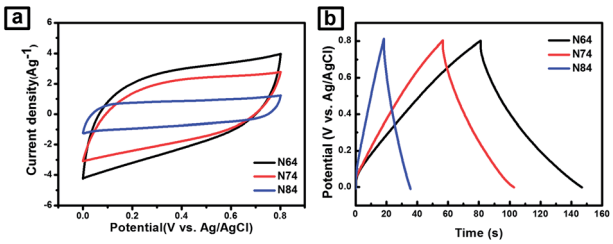

Fig. 4 (a) CVs of TiO_xN_y sheets with a scan rate of 30 mV s^{-1} and (b) constant current charge/discharge curves of TiO_xN_y sheets at a current density of 1.25 A g^{-1}.

suggest a high coulombic efficiency and acceptable reversibility of TiO_xN_y, as shown in Fig. 4b. This figure reveals that the discharge time of N64 is greater than that of the other electrodes. Also, N64 displays the highest specific capacitance 120.9 F g^{-1} at a constant charge/discharge current density of 1.25 A g^{-1}, which is comparable to that of other TiN structures, including nanowires (123 F g^{-1}, 1 M KOH, 10 mV s^{-1})[12] and nanofibers (145 F g^{-1}, 1 M KOH, 2 mV s^{-1}).[14] This good performance is likely owing to the porous structure and the presence of divalent titanium cations in TiO_xN_y. The large specific surface area with numerous active and accessible sites for the absorption enhances the double-layer supercapacitance. Moreover, the coexistence of di- and tri-valent titanium cations in TiO_xN_y offers the extra oxidation of Ti^{2+} to Ti^{3+}, while there is only Ti^{3+} to Ti^{4+} in the TiN electrode, which improves the pseudocapacitance of TiO_xN_y. The stability of N64 is tested in CV with a scan rate of 70 mV s^{-1} for 300 cycles (Fig. S11†). The specific capacitance of the electrode reveals a decay of 12% after 300 cycles. The acceptable electrochemical behavior suggests the feasibility of using TiO_xN_y as a potential electrode material for further electrochemical applications (Fig. S9 and S10† show the CV and GV curves of TiO_xN_y sheets at various scan rates and current densities, respectively).

Conclusions

This work developed a simple method to fabricate freestanding TiO_xN_y sheets *via* the nitridation of numerous interlacing titanate fibers. The conductivity and oxidation state of TiO_xN_y sheets were controlled by the nitridation temperature and reaction time. Additionally, the significant morphological change caused by the O/N atom replacement was related to the formation and ruin of nanopores (2–15 nm) over fibers. Moreover, the high surface area and mixed-oxidation state of Ti cations contribute to charge storage during the interfacial electrochemical reactions. Furthermore, the TiO_xN_y sheet exhibited a specific capacitance of 120.9 F g^{-1} at a current density of 1.25 A g^{-1} in 2 M H_2SO_4.

Acknowledgements

The authors would like to thank the National Science Council of the Republic of China, Taiwan, for financially supporting this research under Contract no. NSC 101-2113-M-007-012-MY3. Ted Knoy is appreciated for his editorial assistance.

Notes and references

1 M. Drygaś, C. Czosnek, R. T. Paine and J. F. Janik, *Chem. Mater.*, 2006, **18**, 3122.
2 M. Zukalova, J. Prochazka, Z. Bastl, J. Duchoslav, L. Rubacek, D. Havlicek and L. Kavan, *Chem. Mater.*, 2010, **22**, 4045.
3 W. Wang, O. Savadogo and Z.-F. Ma, *Int. J. Hydrogen Energy*, 2012, **37**, 7405.
4 Y.-J. Wei, C.-W. Peng, T.-M. Cheng, H.-K. Lin, Y.-L. Chen, C.-Y. Lee and H.-T. Chiu, *ACS Appl. Mater. Interfaces*, 2011, **3**, 3804.
5 H. Kiyono, T. Tsumura, T. Kiyo, M. Toyoda and S. Shimada, *Ceram. Int.*, 2011, **37**, 1813.
6 H. Han, T. Song, J.-Y. Bae, L. F. Nazar, H. Kim and U. Paik, *Energy Environ. Sci.*, 2011, **4**, 4532.
7 P. K. A. G. Mangamma, R. Nithya, T. N. Sairam, V. K. Mittal, M. Kamruddin, S. Dash and A. K. Tyagi, *J. Phys. D: Appl. Phys.*, 2007, **40**, 4597.
8 D. Sun, J. Lang, X. Yan, L. Hu and Q. Xue, *J. Solid. State Chem.*, 2011, **184**, 1333.
9 S. Dong, X. Chen, L. Gu, X. Zhou, H. Xu, H. Wang, Z. Liu, P. Han, J. Yao, L. Wang, G. Cui and L. Chen, *ACS Appl. Mater. Interfaces*, 2010, **3**, 93.
10 J.-H. Kim, K. Zhu, Y. Yan, C. L. Perkins and A. J. Frank, *Nano Lett.*, 2010, **10**, 4099.
11 D. Choi and P. N. Kumta, *J. Electrochem. Soc.*, 2006, **153**, A2298.
12 X. Lu, G. Wang, T. Zhai, M. Yu, S. Xie, Y. Ling, C. Liang, Y. Tong and Y. Li, *Nano Lett.*, 2012, **12**, 5376.
13 R. L. Porto, R. Frappier, J. B. Ducros, C. Aucher, H. Mosqueda, S. Chenu, B. Chavillon, F. Tessier, F. Cheviré and T. Brousse, *Electrochim. Acta*, 2012, **82**, 257.
14 X. Zhou, C. Shang, L. Gu, S. Dong, X. Chen, P. Han, L. Li, J. Yao, Z. Liu, H. Xu, Y. Zhu and G. Cui, *ACS Appl. Mater. Interfaces*, 2011, **3**, 3058.
15 Y. Yue, P. Han, X. He, K. Zhang, Z. Liu, C. Zhang, S. Dong, L. Gu and G. Cui, *J. Mater. Chem.*, 2012, **22**, 4938.
16 W. Smith, H. Fakhouri, J. Pulpytel, S. Mori, R. Grilli, M. A. Baker and F. Arefi-Khonsari, *J. Phys. Chem. C*, 2012, **116**, 15855.
17 M. F. El-Kady, V. Strong, S. Dubin and R. B. Kaner, *Science*, 2012, **335**, 1326.
18 H. Zhang, Y. Chen, W. Wang, G. Zhang, M. Zhuo, H. Zhang, T. Yang, Q. Li and T. Wang, *J. Mater. Chem. A*, 2013, **1**, 8593.
19 X. Zhang, T. Zhang, J. Ng and D. D. Sun, *Adv. Funct. Mater.*, 2009, **19**, 3731.
20 W. Dong, A. Cogbill, T. Zhang, S. Ghosh and Z. R. Tian, *J. Phys. Chem. B*, 2006, **110**, 16819.
21 M. D. Banus, T. B. Reed and A. J. Strauss, *Phys. Rev. B: Solid State*, 1972, **5**, 2775.
22 K. S. W. Sing, D. H. Everett, R. A. W. Haul, L. Moscou, R. A. Pierotti, J. Rouquerol and T. Siemieniewska, *Pure Appl. Chem.*, 1985, **57**, 60.
23 S. A. Sherrill, J. Duay, Z. Gui, P. Banerjee, G. W. Rubloff and S. B. Lee, *Phys. Chem. Chem. Phys.*, 2011, **13**, 15221.
24 Y. Qiu and L. Gao, *J. Phys. Chem. B*, 2005, **109**, 19732.